Journal of Magnetic Resonance 200 (2009) 251–260

Contents lists available at ScienceDirect

Journal of Magnetic Resonance

journal homepage: www.elsevier.com/locate/jmr

Double-quantum homonuclear NMR correlation spectroscopy of quadrupolar nuclei subjected to magic-angle spinning and high magnetic field

Q. Wang [a,b,c], B. Hu [a], O. Lafon [a], J. Trébosc [a], F. Deng [b,*], J.P. Amoureux [a,*]

[a] UCCS, CNRS-8181, Lille University, Fr-59652, Villeneuve d'Ascq, France
[b] State Key Laboratory of Magnetic Resonance and Atomic and Molecular Physics, Wuhan Center for Magnetic Resonance, Wuhan Institute of Physics and Mathematics, Chinese Academy of Sciences, Wuhan 430071, China
[c] Graduate School of the Chinese Academy of Sciences, Beijing, China

ARTICLE INFO

Article history:
Received 27 April 2009
Revised 6 July 2009
Available online 14 July 2009

Keywords:
Solid-state NMR
Half-integer quadrupolar nuclei
Fast MAS
Double-quanta spectroscopy

ABSTRACT

We present a new application of the $R2_2^1$ symmetry-based dipolar recoupling scheme, for exciting directly double-quantum (2Q) coherences between the central transition of homonuclear half-integer quadrupolar nuclei. With respect to previously published 2Q-recoupling methods (M. Eden, D. Zhou, J. Yu, Chem. Phys. Lett. 431 (2006) 397), the $R2_2^1$ sequence is used without π/2 bracketing pulses and with an original super-cycling. This leads to an improved efficiency (a factor of two for spin-5/2) and to a much higher robustness to radio-frequency field inhomogeneity and resonance offset. The 2Q-coherence excitation performances are demonstrated experimentally by ^{27}Al NMR experiments on the aluminophosphates berlinite, VPI5, $AlPO_4$-14, and $AlPO_4$-CJ3. The two-dimensional 2Q–1Q correlation experiments incorporating these recoupling sequences allow the observation of 2Q cross-peaks between central transitions, even at high magnetic field where the difference in offset between octahedral and tetrahedral ^{27}Al sites exceeds 10 kHz.

1. Introduction

Solid-state nuclear magnetic resonance (SS NMR) spectroscopy is a powerful tool for the investigation of materials. Magic-angle spinning (MAS) enhances spectral resolution by largely removing the effects of anisotropic spin interactions, such as chemical shift anisotropy (CSA) and dipolar couplings. However, the through-space dipolar couplings encode important information on the spatial proximity of atoms through their inverse cubic dependence on the inter-nuclear distance. Therefore, dedicated radio-frequency (rf) pulse sequences have been developed to specifically reintroduce these interactions under the MAS conditions [1,2]. In particular, homonuclear recoupling sequences restore dipolar interactions between nuclei of the same isotopic type. Nevertheless, most of homonuclear recoupling schemes are dedicated to the case of spin-1/2 nuclei, whereas about two thirds of NMR active, stable nuclei have larger half-integer spin values (e.g. $S = 3/2$: ^{11}B, ^{23}Na; $S = 5/2$: ^{17}O, ^{27}Al).

Homonuclear dipolar recoupling of quadrupolar nuclei under MAS is difficult because of the intricate nuclear spin dynamics of the quadrupolar nuclei in the presence of rf fields and sample rotation. Therefore, dipolar recoupling in quadrupolar systems was first achieved without the application of rf-field. Indeed, the MAS averaging of homonuclear couplings can be prevented by interferences between homonuclear dipolar couplings and another anisotropic interaction, such as heteronuclear dipolar coupling with protons [3,4] or quadrupolar interactions [5–12]. Rotational resonance (R^2) has also been demonstrated [13]. However, these recoupling phenomena under the absence of the rf-field occur only in a limited range of MAS frequency and their efficiencies are low for an extended range of resonance frequencies [7,9]. Off-magic-angle spinning prevents the averaging of dipolar interactions but entails resolution decrease, except when employing dynamic angle spinning (DAS) methods [14,15].

In case of half-integer nuclei, the application of weak (selective) rf pulses allows rotating the central transition (CT) coherence between energy levels −1/2 and 1/2 in the same fashion as for fictitious spin-1/2 nuclei [16]. For rf amplitudes much smaller than the quadrupolar coupling, the CT nutation frequency of spin-S is $\nu_{\mathrm{nut}}^{\mathrm{CT}} = (S + 1/2)\nu_1$. Even if the fictitious spin-1/2 approximation may not be fulfilled at all times for all crystallite orientations in a powder, the dipolar recoupling techniques employing rf fields that were originally introduced for spins-1/2 were transposed to the case of half-integer quadrupolar nuclei. Rotary resonance recoupling (R^3) techniques and especially the HORROR condition [17,18] have been demonstrated for recoupling of quadrupolar nuclei [19–23]. The HORROR condition, which selectively

* Corresponding authors. Tel.: +33 3 20 43 41 43; fax: +33 3 20 43 68 14 (J.P. Amoureux).
E-mail addresses: dengf@wipm.ac.cn (F. Deng), jean-paul.amoureux@univ-lille1.fr (J.P. Amoureux).

1090-7807/$ - see front matter © 2009 Elsevier Inc. All rights reserved.
doi:10.1016/j.jmr.2009.07.009

reintroduces the homonuclear dipolar interaction, is obtained for a spin-S when the rf amplitude ν_1 fulfills:

$$\nu_1 = \nu_R/(2S+1) \quad (1)$$

where ν_R is the MAS frequency. Recently, it was shown that symmetry-based pulse sequences display superior rf error tolerance than the HORROR recoupling [24–27]. These symmetry-based pulse sequences were incorporated into 2D experiments, which correlate 2Q-coherences (2QCs) with the respective CT single-quantum (1Q) coherences within each spin-pair [25]. Compared to 1Q–1Q correlation experiments, the 2Q–1Q correlation spectroscopy benefits from the increased frequency dispersion of 2QCs and the possibility to probe correlation between equivalent sites. These symmetry-based recoupling methods have been integrated into 1D 2Q filtering (2QF) experiments in order to measure inter-nuclear distances and to analyze the relative orientations of quadrupolar and dipolar tensors [28], and it was concluded that 'analysis of 2Q filtered curves of quadrupolar nuclei is feasible if some prior knowledge on dipolar and/or quadrupolar interactions is available'. Very recently [57], it has also been shown that these two relative orientations could been obtained directly by fitting the line-shapes observed in 2D 2Q–1Q spectra, even with powder samples. The symmetry-based pulse sequences were also used in case of double-rotation (DOR) experiments by synchronizing the rf pulses with the outer rotation of the sample and this allowed obtaining 2D 2Q–1Q spectra with high-resolution in both dimensions for ^{23}Na and ^{27}Al nuclei [29].

However, all existing 2Q-recoupling sequences suffer from a large sensitivity to offsets and to rf-field missetting and inhomogeneity. This is a direct consequence of the low rf amplitudes required to minimize CT signal losses during the recoupling and the requirement that the rf amplitude satisfies Eq. (1). The restricted bandwidths set practical limitations on uniform 2QC excitation of samples exhibiting large frequency dispersion (e.g. ^{27}Al), because of chemical or quadrupolar shifts. The chemical shift dispersion is especially critical for NMR studies in high magnetic fields. The low tolerance to rf errors requires the use of volume-restricted rotors, thus decreasing the achievable sensitivity. The purpose of this article is to propose a new application of the $R2_2^1$ symmetry-based sequence, which reduces both limitations for homonuclear dipolar 2Q-excitation and reconversion.

2. Pulse sequence

2.1. 1D 2QF experiment and 2D 2Q–1Q spectroscopy

Fig. 1a depicts the pulse scheme, which has been mainly employed so far to record 2D 2Q–1Q correlation spectra on half-integer quadrupolar nuclei [22,25,27]. Homonuclear 2QCs were excited by partly zero-quantum (0Q) recoupling sequences that were bracketed by two CT-selective $\pi/2$ pulses. These bracketing $\pi/2$ pulses achieve the conversion of the 0Q recoupling sequences into 2Q schemes. The bracketed recoupling methods allow the excitation of 2QCs from longitudinal magnetization. The excited 2QCs are subjected to a CT-selective π-pulse, which is phase-cycled to eliminate all 2QC involving a single nucleus through its satellite transitions (Fig. 1c) [22]. The 2QCs are reconverted into longitudinal CT polarization by repeating the excitation pulse sequence with a phase-shift of $\pi/2$ [2]. Finally the CT-selective $\pi/2$ read-pulse creates observable 1Q coherences. Maximal sensitivity is obtained when the excitation and reconversion delays are equal. These delays are denoted τ in the following.

For 1D 2QF experiment (see numerical simulations of Figs. 2–5 and experimental results of Fig. 6 and 7), the CT-selective π-pulse is inserted between two equal short delays [25]. For 2D 2Q–1Q spectra (see Figs. 8–10), the delays around the central pulse are replaced by unequal incremented time periods, qt_1 and $(1-q)t_1$. [22]. The position of the CT-selective π-pulse allows scaling the chemical and quadrupolar shifts in the indirect dimension F_1, such that the scaled CT 2QC frequency is $(1-2q)(\nu_j+\nu_k)$, where ν_j and ν_k are the CT 1Q frequencies of the connected two species.

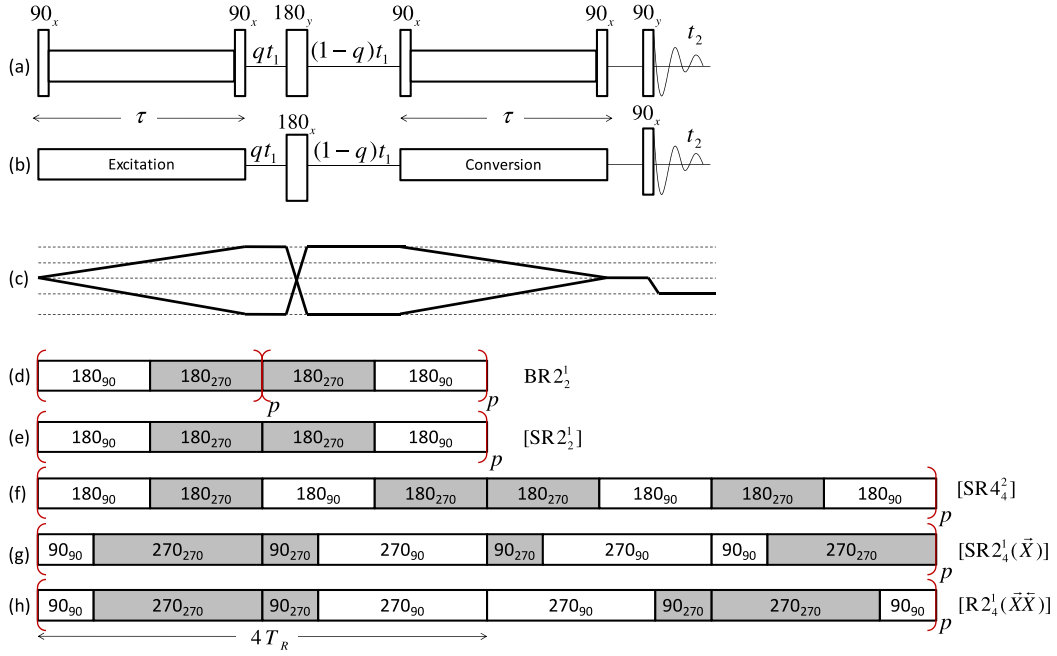

Fig. 1. 2Q–1Q pulse sequences using bracketed (a) or unbracketed (b) homonuclear dipolar recoupling schemes. All rf pulses depicted in the figure are CT-selective. The selected coherence transfer pathway is shown in (c). The DQ single-spin signal is cancelled by the CT-selective π-pulse and only spin-pair DQ coherences result in observable signal. The q parameter is used to scale *all* interactions in order to avoid folding of the resonances along the F_1 dimension. Recoupling schemes used in this article with either sequence (b): $BR2_2^1(\pi)$ (d), or sequence (a): $[SR2_2^1(\pi)]$ (e), $[SR4_4^2(\pi)]$ (f), $[SR2_4^1(X)]$ (g) or $[R2_4^1(\vec{X}\bar{\vec{X}})]$ (h). They use either simple (d–f), or composite (g and h) π-pulses. Phases are equal to 90 or 270°, according to the pulse is shown in white or grey. The recoupling schemes use two types of super-cycling: (d) an overall phase shift from the middle of τ delay, or (e–h) a succession of $SRN_n^{N/2}$ blocks that last either $4T_R$ (e) or $8T_R$ (f–h).

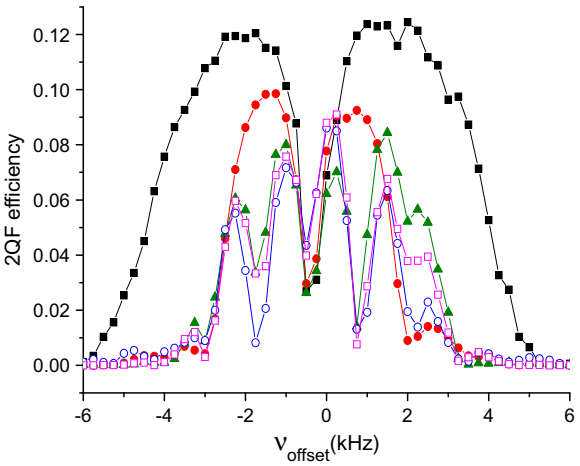

Fig. 2. Simulations of 2QF efficiency of the 'diagonal' peak ($\Delta = 0$) with $F_1 = 2(1-2q)F_2$, versus resonance offset, ν_{offset}, at Larmor frequency $\nu_0 = 208.6$ MHz and a MAS frequency $\nu_R = 15$ kHz. The spin system consists of two ^{27}Al nuclei ($S = 5/2$) with quadrupolar parameters, $C_Q = 4.07$ MHz and $\eta_Q = 0.43$. The dipolar coupling between them was $b_{12} = -95$ Hz. The rf nutation frequency for the recoupling sequence was fixed to $\nu_1 = 2.5$ kHz. The pulse lengths for the central π and the four bracketing $\pi/2$ pulses are 25 and 12.5 μs, respectively. Different homonuclear recoupling sequences were employed: black full squares (■): $BR2_2^1$ (π) with $\tau = 2933$ μs, red full dots (●): [$SR2_2^1$ (π)] with $\tau = 2133$ μs, green full triangles (▲): [$SR4_4^2$ (π)] with $\tau = 2666$ μs, red empty squares (□) [$R2_4^1$ ($\bar{X}\,\bar{X}$)] with $\tau = 2133$ μs, and blue empty dots (○) [$SR2_4^1$ ($\bar{X}$)] with $\tau = 2133$ μs (For interpretation of color mentioned in this figure, the reader is referred to the web version of this article.).

Furthermore, as the homonuclear recoupling sequences are not γ-encoded [2,18], the t_1 evolution period must be incremented in steps of integer number of rotor period, τ_R, thus leading to a limited spectral width in F_1 [25]. However, any folding in F_1 can be avoided by using an appropriate scaling, i.e. an appropriate q value.

However, an important limitation of the application of rf pulse sequences to half-integer quadrupolar nuclei is the difficulty to selectively control the central-transition polarization. Hence, in the design of pulse sequences dedicated to half-integer quadrupolar nuclei, we must endeavor to limit the number of rf pulses in order to increase the sensitivity. Following this general principle, we employ sequences that achieve 2Q-recoupling but does not require any bracketing $\pi/2$-pulse [25]. This possibility was first demonstrated by Edén and co-workers when introducing $R2_2^1$ recoupling methods but was not further exploited [25]. To the best of our knowledge, only one 2QF 1D spectrum of α-Al_2O_3 recorded without bracketing $\pi/2$-pulse has been presented in the literature [25]. In the present article, we further investigate the potentialities of this unbracketed recoupling method. The corresponding pulse scheme for 2D 2Q–1Q spectroscopy of half-integer spin nuclei is depicted in Fig. 1b. Timing and phase-cycling are identical to those used for the sequence of Fig. 1a. Hence the coherence transfer pathways are still those displayed in Fig. 1c. The main differences between the methods introduced in Ref. [25] and in the present article lye in the absence of bracketing $\pi/2$ pulses and in the super-cycle of the recoupling sequences. The super-cycle we use is similar to that described by Mali et al. [22] and corresponds to a global phase-reversal at the midpoint of the τ intervals. These two simultaneous differences yield higher efficiency and robustness than previous methods. The design and the super-cycle of the employed recoupling methods are presented in the next subsection.

2.2. Homonuclear dipolar recoupling

In this work, RN_n^ν-based [2,30] recoupling schemes are employed. They are composed of N/2 $R_\varphi R_{-\varphi}$ inversion cycle pairs, where R is an inversion element of duration nT_R/N and φ indicates an overall phase-shift of $\nu\pi/N$. Here, R either represents a simple π_0-pulse (Fig. 1d–f) or the composite inversion pulses $\vec{X} = (\pi/2)_0(3\pi/2)_\pi$ (Fig. 1g and h) and $\overleftarrow{X} = (3\pi/2)_\pi(\pi/2)_0$. (Fig. 1h), which are both internally compensated to resonance offsets and rf errors. The RN_n^ν sequences built from the basic elements are denoted $RN_n^\nu(\pi)$ and $RN_n^\nu(\vec{X})$ in the following.

Several RN_n^ν symmetries were tested for the dipolar recoupling of half-integer quadrupolar nuclei. $R4_4^1$ and $R6_6^2$ symmetries achieve zero-quantum (0Q) dipolar recoupling and suppress all other dipolar and shielding terms [2,24,25]. Therefore, they must be bracketed by CT-selective $\pi/2$ pulses in order to excite 2QC and they can only be employed with the pulse sequence of Fig. 1a [25]. In contrast, $RN_N^{N/2}$ (π or $\vec{X}$) and $R2_4^1$ (π or $\vec{X}$) pulse sequences (Fig. 1d–h) generate a dipolar average Hamiltonian (AH) between homonuclear spins j and k, which comprises both 0Q and 2Q operators [25]. The expression of the AH corresponding to the different sequences described in this article (Eq. (2) and (3)) has been given in ref [25], and it is only introduced here for the reader convenience. The recoupling sequences described in Fig. 1d–h provide both 0Q and 2Q-recoupling and the corresponding AH is equal to:

$$H = b_{jk} f(\beta_R, \gamma_R)\{S_j^+ S_k^+ + S_j^- S_k^- - 4S_{jz}S_{kz} + S_j^+ S_k^- + S_j^- S_k^+\} \quad (2)$$

In the above equation, b_{jk} is the dipolar coupling constant and $f(\beta_R, \gamma_R) = 3\sin(2\beta_R) \cdot \cos\gamma_R / (16\sqrt{2})$ is a function of Euler angles (β_R, γ_R) describing the orientation of the inter-nuclear vector in the rotor-fixed frame. Eq. (2) shows that $RN_N^{N/2}$ and $R2_4^1$ schemes can be incorporated in the pulse sequences of Fig. 1b, since the 2Q terms, $S_j^+ S_k^+ + S_j^- S_k^-$, enable direct excitation of 2QC from longitudinal magnetization. $RN_N^{N/2}$ and $R2_4^1$ symmetries do not suppress all shielding terms [25,27]. However, these undesirable AH terms can be suppressed by the $SRN_n^\nu = RN_n^\nu RN_n^{-\nu}$ phase inversion super-cycle, while the average dipolar Hamiltonian is not affected and hence Eq. (2) remains valid [2,31,32]. As discussed in Ref. [25] and [27], the super-cycled sequences $SRN_N^{N/2}$ and $SR2_4^1$ can also be incorporated in the pulse sequence of Fig. 1a in order to convert the 0Q operators in Eq. (2) into pure 2Q operators. These $\pi/2$-bracketed sequences are denoted [$SRN_N^{N/2}$] and [$SR2_4^1$] in the following. Their AH is equal to:

$$[H] = 2b_{jk} f(\beta_R, \gamma_R)\left\{S_j^+ S_k^+ + S_j^- S_k^-\right\} \quad (3)$$

disregarding the quadrupolar interaction.

The performances of $\pi/2$-bracketed recoupling schemes have already been compared by Edén and co-workers in the context of ^{23}Na ($S = 3/2$) and ^{27}Al ($S = 5/2$) homonuclear correlations [25,27]. In Ref. [25], they showed that the [$SR2_2^1$ (π)] sequence (Fig. 1a and e) is more efficient and more robust to offsets and rf-field inhomogeneity than [$SR4_4^1$ (π)], [$SR6_6^2$ (π)] and [HORROR] sequences. Very recently, they demonstrated that [$SR4_4^2$ (π)] scheme outperforms [$SR2_2^1$ (π)], [$SR2_4^1$ ($\bar{X}$)] and [$R2_4^1$ ($\bar{X}\,\bar{X}$)] (a short name for [$R2_4^1(\bar{X})$ $R2_4^1(\bar{X})$]) sequences in terms of optimum 2QF efficiencies for ^{23}Na and ^{27}Al nuclei, whereas [$SR2_4^1$ ($\bar{X}$)] and [$R2_4^1$ ($\bar{X}\,\bar{X}$)] sequences manifest higher robustness to both resonance offsets and rf-field inhomogeneity.

However, it was noticed that the 2QF efficiency drops significantly versus offsets, even for small differences in the CT frequencies. This prevents the observation of cross-peaks between sites exhibiting large differences in isotropic chemical shifts. To reduce this problem, we explore here an unbracketed $R2_2^1$ -based recoupling scheme employing a simple π_0-pulse as basic element. Edén and co-workers showed the possibility of 2QC excitation of quadrupolar spins by using unbracketed $SR2_2^1$ (π) recoupling method. However, they obtained a lower 2QF efficiency for the unbracketed sequence than for the bracketed version [$SR2_2^1$ (π)] [25]. This

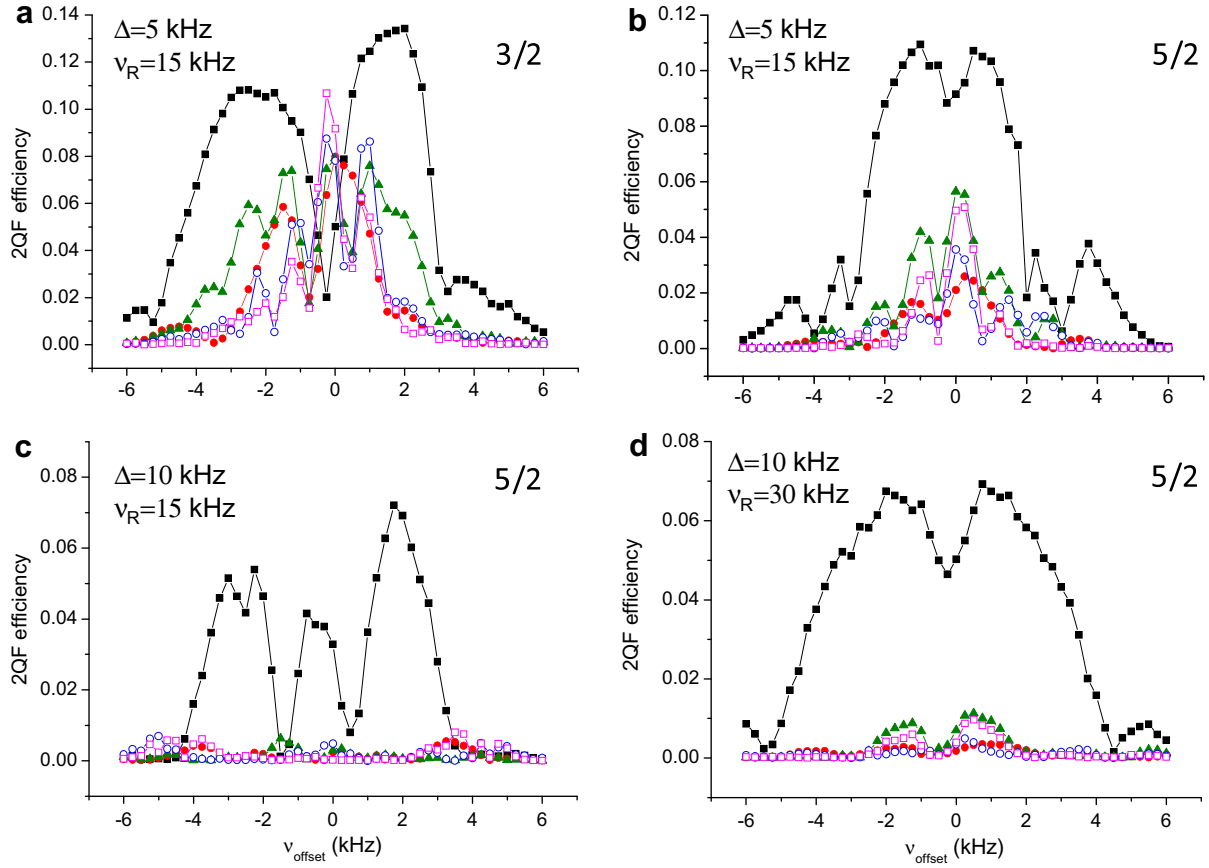

Fig. 3. Simulations of 2QF efficiency of cross-peaks ($\Delta \neq 0$) versus resonance offset, ν_{offset}. (a) The spin system consists of two ^{23}Na nuclei ($S = 3/2$) with quadrupolar parameters $C_Q = 2.6$ MHz, $\eta_Q = 0.6$, and a dipolar coupling constant $b_{12} = -259$ Hz. The Larmor frequency was $\nu_0 = 105.8$ MHz and the MAS frequency $\nu_R = 15$ kHz. The frequency separation between the two sites was $\Delta = 5$ kHz. The rf nutation frequency for the recoupling sequence was $\nu_1 = 3.75$ kHz. (b–d) The spin system consists of two ^{27}Al nuclei ($S = 5/2$), and its parameters are identical to those of Fig. 2, except the frequency separation, the MAS frequency and the rf nutation frequency, which are as follows: (b) $\Delta = 5$ kHz, $\nu_R = 15$ kHz, $\nu_1 = 2.5$ kHz, (c) $\Delta = 10$ kHz, $\nu_R = 15$ kHz, $\nu_1 = 2.5$ kHz, (d) $\Delta = 10$ kHz, $\nu_R = 30$ kHz, $\nu_1 = 5$ kHz. Symbols for the different recoupling schemes are identical to those defined for Fig. 2.

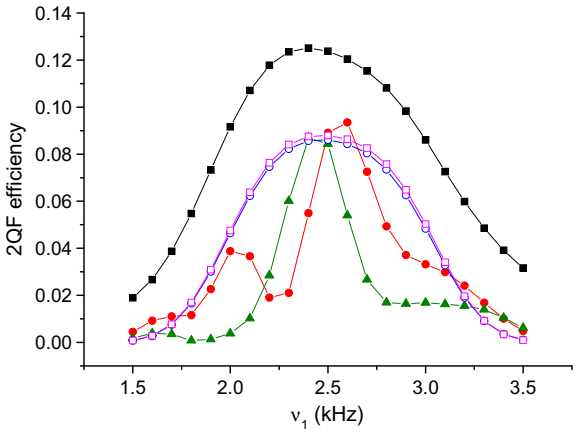

Fig. 4. Simulations of 2QF efficiency of the 'diagonal' peak ($\Delta = 0$), versus the rf nutation frequency, ν_1. The spin system consists of two ^{27}Al nuclei ($S = 5/2$). The carrier frequency is optimized for maximum nominal ($\nu_1 = 2.5$ kHz) sensitivity: $\nu_{offset} = 0$ for $[R2^1_4(\bar{X}\,X)]$ and $[SR2^1_4(\bar{X})]$ sequence, 1 kHz for $BR2^1_2(\pi)$ and $[SR2^1_2(\pi)]$ sequences, 1.5 kHz for $[SR4^2_4(\pi)]$ sequence. All other parameters and symbols are identical to those employed in Fig. 2.

can result from the super-cycle as well as the recoupling time, which was optimized for the unbracketed version. In this article, we investigate the unbracketed $R2^1_2$ sequence employing a super-cycle, which consists in a phase inversion from the middle of the τ delay. This original super-cyle, depicted in Fig. 1d, better eliminates the offset and rf error dependence than the usual phase inversion super-cycle, $SR2^1_2 = R2^1_2R2^{-1}_2$. It will be denoted $BR2^1_2$ in the following. When the excitation and reconversion intervals span 4p rotor periods, the $BR2^1_2(\pi)$ sequence corresponds to $(R2^1_2)_p(R2^{-1}_2)_p = R2p^p_{2p}R2p^{-p}_{2p}$ symmetry. The better performances of $BR2^1_2$ super-cycling compared to phase inversion super-cycling cannot be explained by the selection rules on the zero- and first-order AH and are not yet fully understood [31]. In this article, we compare the performances of $BR2^1_2(\pi)$ recoupling sequence with those of previously reported sequences, $[SR2^1_2(\pi)]$, $[SR4^2_4(\pi)]$, $[SR2^1_4(\bar{X})]$ and $[R2^1_4(\bar{X}\,X)]$.

3. Simulations

In preparation for the experiments, we performed simulations with the SIMPSON software [33], and the powder averaging was performed using 168 crystallites following the REPULSION algorithm [34]. The computing time is approximately proportional to the cube of the size of the density matrix describing the spin system. Therefore, to limit the computing time to a few days for each figure, we have restricted our spin-system to only two interacting nuclei of spin-3/2 or -5/2. We have chosen to use two identical sites with the same quadrupolar parameters, and hence the same powder line-shapes, but with symmetrical isotropic chemical shifts of $\pm\Delta/2$ with respect to the reference frequency. The gravity

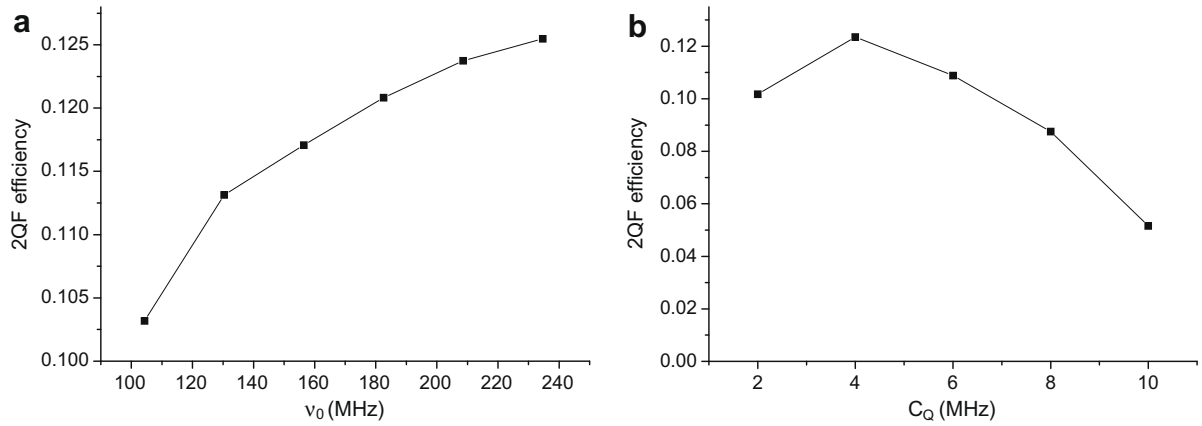

Fig. 5. Simulations of $BR2_2^1$ (π) 2QF efficiency of the 'diagonal' peak ($\Delta = 0$), versus (a) the Larmor frequency ν_0 ($C_Q = 4.07$ MHz) and (b) the C_Q value ($\nu_0 = 208.6$ MHz). The carrier frequency is fixed at $\nu_{offset} = 1$ kHz, $\nu_R = 15$ kHz, $\eta_Q = 0.43$.

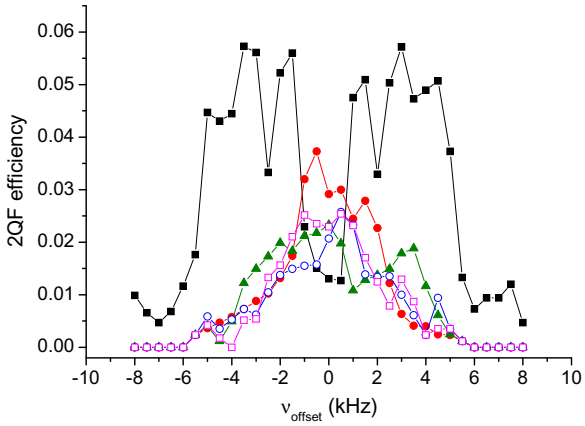

Fig. 6. Experimental ^{27}Al 2QF efficiency of the 'diagonal' peak ($\Delta = 0$) versus the resonance offset. The experiments were performed at $\nu_0 = 208.6$ MHz and $\nu_R = 15$ kHz on berlinite powder. The rf nutation frequency for the homonuclear recoupling sequence was $\nu_1 \approx 2.5$ kHz. The rf-power for the central π and the four bracketing $\pi/2$ pulses is 7.9 kHz. The excitation time τ for $BR2_2^1$ (π), [$SR2_2^1$ (π)], [$SR4_4^2$ (π)], [$R2_4^1$ ($\bar{X}\,X$)] and [$SR2_4^1$ ($\bar{X}$)] are 1866, 1333, 1066, 1066 and 1066 μs. All other parameters and symbols are identical to those employed in Fig. 2.

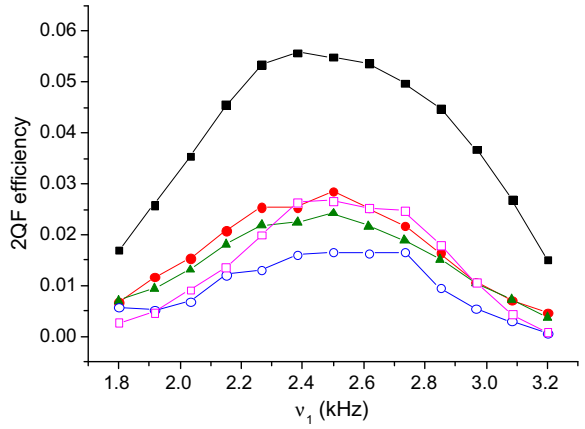

Fig. 7. Experimental ^{27}Al 2QF efficiency of the 'diagonal' peak ($\Delta = 0$) versus the rf nutation frequency. The experiments were performed at $\nu_0 = 208.6$ MHz and $\nu_R = 15$ kHz on berlinite powder. The employed resonance offsets, ν_{offset}, were fixed to the values that for each recoupling sequence provided the optimum 2QF efficiency in Fig. 6. All other parameters and symbols are identical to those employed in Fig. 6.

centers of these line-shapes are shifted from the isotropic chemical shift values by the quadrupolar induced shifts ($\nu_{QIS} < 0$), and they thus appear at $\pm\Delta/2 + \nu_{QIS}$. The rf-carrier is defined with respect to the reference frequency through the off-resonance frequency (ν_{offset}), which means that the frequency differences between the rf irradiation and the isotropic chemical shifts (or the line-shape gravity centers) are equal to $\pm\Delta/2 - \nu_{offset}$ (or to $\pm\Delta/2 - \nu_{offset} + \nu_{QIS}$). The spinning speed was always fixed to $\nu_R = 15$ kHz (except in Fig. 3d), and the quadrupolar and dipolar parameters of the two-spin system are those of ^{23}Na in Na_2SO_4 for spin-3/2 nuclei ($C_Q = 2.6$ MHz, $\eta_Q = 0.6$, $d_{12} = 318$ pm, $b_{12} = -259$ Hz) and of ^{27}Al in $AlPO_4$ berlinite for spin-5/2 nuclei ($C_Q = 4.07$ MHz, $\eta_Q = 0.43$, $d_{12} = 440$ pm, $b_{12} = -95$ Hz) (except in Fig. 5b). In both cases, the inter-nuclear vector was assumed aligned with the z principal axis of the quadrupolar tensor.

We ran simulations on a two-spin system, denoted S_1 and S_2 in the following. We detected the magnetization transferred from S_1 to S_2 during the 2QF experiment. It corresponds to one of the two cross-peaks between S_1 and S_2 CT transitions on the 2D 2Q–1Q spectrum. These simulations were done starting from S_1 longitudinal magnetization, i.e. the operator S_{1z}, and detecting only the -1Q coherence of spin-S_2, which corresponds to the operator S_2^-. The transfer efficiency was then calculated in comparison to the signal from a CT-selective 90° pulse on S_2.

3.1. 'Diagonal'-peak, with $F_1 = 2(1 - 2q)F_2$, of two similar nuclei ($\Delta = 0$)

We have first investigated the case of two nuclei with identical chemical shifts, $\Delta = 0$. The 2QF efficiency was calculated by numerical simulations as function of the offset, ν_{offset}, for all sequences described in Fig. 1, and at two different static magnetic fields 9.4 and 18.8 T. The obtained efficiencies correspond to those of auto-peaks situated on the diagonal of the 2D 2Q–1Q spectrum, which has a slope of $2(1 - 2q)$. For spin-3/2 nuclei (results not shown), all recoupling sequences are equivalent in terms of efficiency (around 16% for on-resonance irradiation, $\nu_{offset} = 0$) and robustness to offset. However, the efficiency of diagonal peaks is slightly less sensitive to offsets for $BR2_2^1$ (π) method. In contrast, for spin-5/2 nuclei, the $BR2_2^1$ method displays a higher efficiency and robustness to offset compared to the bracketed sequences. The results obtained at 9.4 (not shown) and 18.8 T (Fig. 2) are very similar. The larger 2QF efficiency for the unbracketed method partly stems from the inability of the bracketing pulses to selectively rotate the central-transition polarization, since the rf pulses do not operate in the CT-selective regime for all crystallites and time

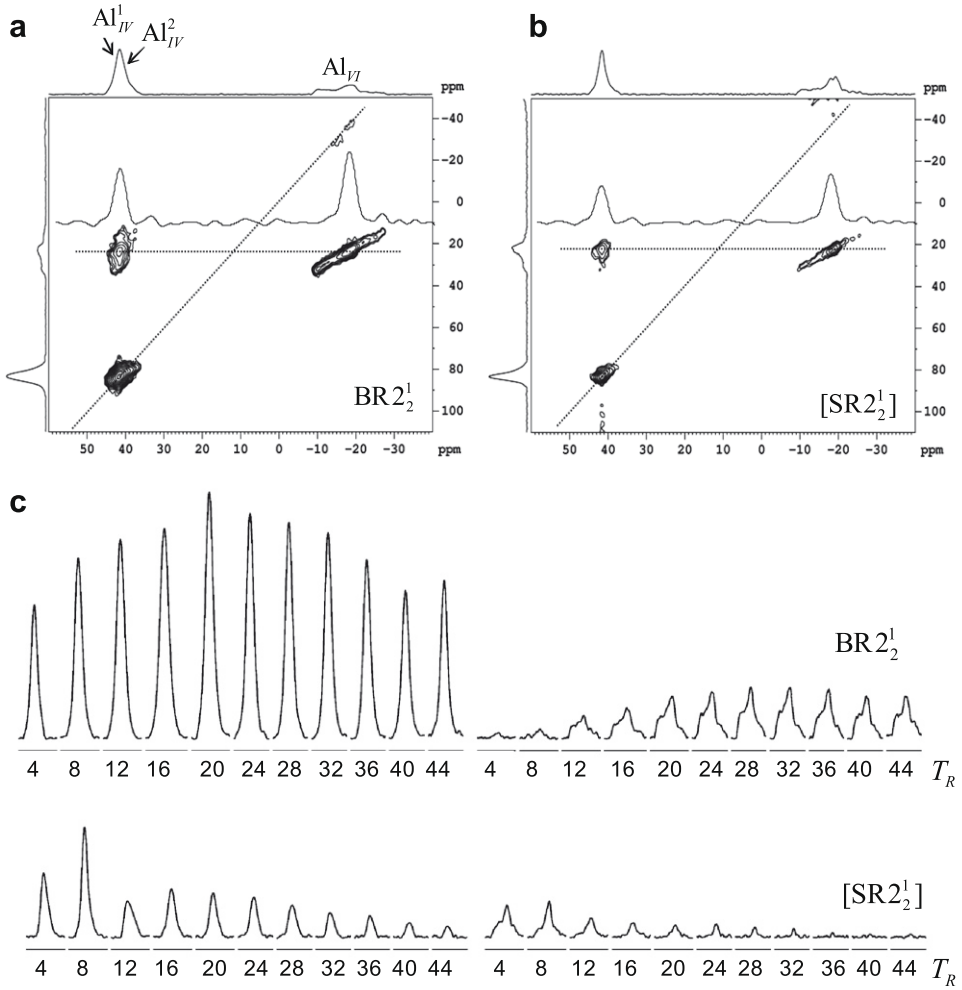

Fig. 8. Experimental 2Q–1Q ^{27}Al correlation spectra of $AlPO_4$-VPI5 at 9.4 T (ν_0 = 104.3 MHz) and ν_R = 13.5 kHz, using (a) $BR2^1_2$ (π) and (b) [$SR2^1_2$ (π)] for 2QC excitation. The parameter q has been fixed to 0.2, and the 2D spectra have been re-scaled along F_1 to restore the actual chemical shift values. The relaxation delay was 0.5 s and the indirect dimension of each spectrum was acquired with 120 points each obtained with 64 scans. The total experimental time for each 2D spectrum was 64 min. The rf nutation frequencies were $\nu_1 \approx 2.25$ kHz for the homonuclear recoupling sequence and 4.17 kHz for the CT-selective π and $\pi/2$ pulses. The excitation and reconversion intervals τ were equal to 2070 μs and 592 μs for $BR2^1_2$ (π) and [$SR2^1_2$ (π)] sequences, respectively. Slices along the cross-peaks ($F_1 \approx 24$ ppm) are also represented. (c) F_1 projections versus τ expressed in number of rotor periods. The left part corresponds to tetrahedral auto-peak ($F_1 \approx 90$ ppm), while the right part corresponds to cross-peaks ($F_1 \approx 24$ ppm).

points. An interesting phenomenon can also be observed in Fig. 2: all sensitivity curves present a narrow dip for on-resonance irradiation. This dip is always observed, whatever may be the relative orientations of the two quadrupolar tensors and the inter-nuclear vector. We do not have presently any explanation for this effect. This dip entails that the carrier frequency must be set up in a frequency region devoid of resonance.

3.2. Cross-peaks of two different nuclei ($\Delta \neq 0$)

We then simulated the case of two nuclei resonating at Δ = 5 kHz from each other. The simulations were performed for spin-3/2 at 9.4 T (Fig. 3a) and spin-5/2 at 18.8 T (Fig. 3b). By comparing Figs. 2 and 3b, we observe that for spin-5/2 nuclei the maximum efficiency of bracketed sequences is roughly divided by a factor of two when increasing the chemical difference from Δ = 0 to 5 kHz, whereas that of $BR2^1_2$ (π) is only slightly decreased. All experiments present one or several dips of sensitivity, which means that for sensitivity reasons, the carrier frequency must be carefully optimized. However, globally, the $BR2^1_2$ sensitivity is much larger and much more robust to offset than bracketed sequences, especially for spin-5/2 nuclei. For spin-3/2 nuclei this chemical shift difference, Δ = 5 kHz, is often an upper limit for most nuclei (e.g. ^{23}Na or ^{11}B), even at high magnetic fields, but this value can be much larger for spin-5/2 nuclei. For example, it can amount to Δ = 10 kHz for the cross-peaks between tetrahedral and octahedral ^{27}Al sites at 18.8 T. Thus we performed the same simulations, with the same spinning speed ν_R = 15 kHz, but we doubled the chemical shift difference: Δ = 10 kHz (Fig. 3c). It can be observed in this figure that the efficiencies obtained for bracketed sequences then become negligible. This is not the case with the $BR2^1_2$ sequence, and even if there are two large dips at $\nu_{offset} \approx 0.5$ and -1.5 kHz, it always remains possible to get a reasonable efficiency (≈ 6–8%) by optimizing the carrier frequency. These two dips disappear when increasing the spinning speed and thus the rf-field. In Fig. 3d, simulated with Δ = 10 kHz and ν_R = 30 kHz, one observes for the $BR2^1_2$ sequence the same maximum efficiency as in Fig. 3c, without the two dips. The spectral width is larger than in Fig. 3b but the increase of isotropic chemical shift difference leads to a 30% decrease in the maximal 2QF efficiency. Simultaneously, the efficiency for the bracketed sequences remains very weak. The observation of 2Q–1Q cross-peaks of half-integer quadrupolar nuclei with large frequency separation thus requires the use of the $BR2^1_2$ sequence under fast MAS.

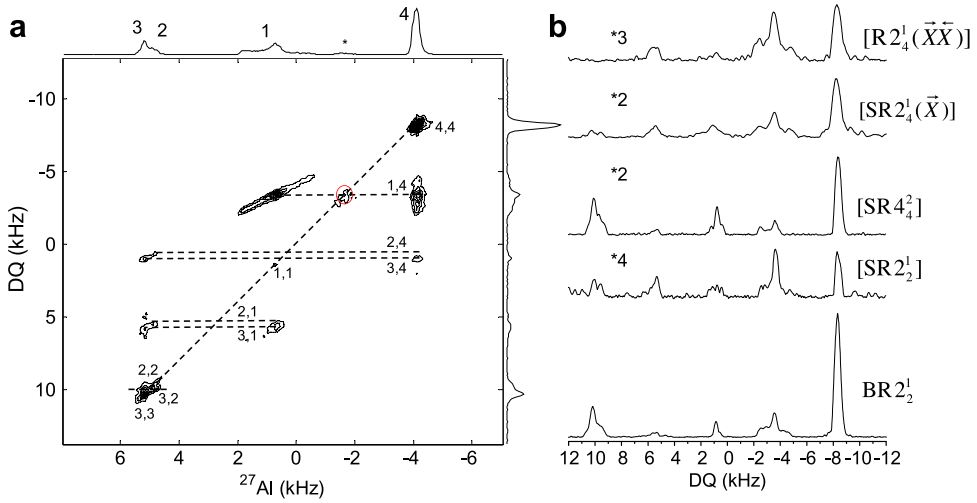

Fig. 9. Experimental ^{27}Al correlation spectra of $AlPO_4$-14 at 18.8 T (ν_0 = 208.6 MHz) and ν_R = 16 kHz. (a) 2Q–1Q 2D spectrum using $BR2^1_2$ (π) for 2QC excitation. The parameter q has been fixed to 0.2, and the spectrum has been re-scaled in the F_1 dimension. The relaxation delay was 0.6s and the indirect dimension of each spectrum was acquired with 140 points each obtained with 192 scans. The total experimental time for each 2D spectrum was 4.5 h. It can be decreased to 2 h, without loss in S/N ratio, by using an initial hyper-secant CT enhancing. The impurity at c.a. −2 kHz is indicated by a star and its auto-peak is circled. The rf nutation frequencies were $\nu_1 \approx 2.67$ kHz for the homonuclear recoupling sequence and 6.67 kHz for the CT-selective π and $\pi/2$ pulses. (b) Comparison of F_1 projections for the five homonuclear recoupling sequences described in Fig. 1. The excitation time τ for $BR2^1_2$ (π), $[SR2^1_2$ (π)], $[SR4^2_4$ (π)], $[R2^1_4$ ($\vec{X}\,\vec{X}$)] and $[SR2^1_4$ ($\vec{X}$)] are 1250, 750, 1000, 1000 and 1000 μs.

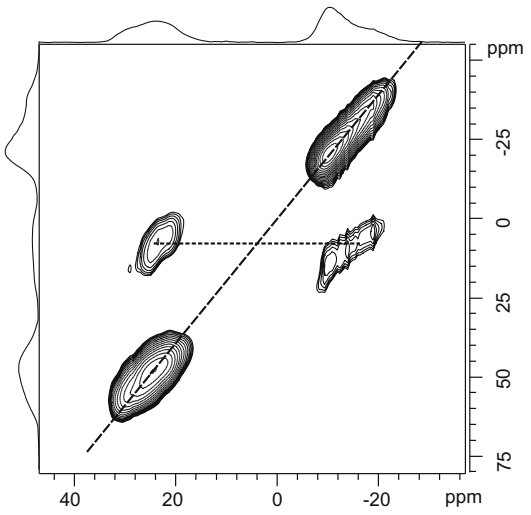

Fig. 10. Experimental 2Q–1Q ^{27}Al correlation spectrum of $AlPO_4$-CJ3 at ν_0 = 78.16 MHz and ν_R = 12.5 kHz, using $BR2^1_2$ (π) for 2QC excitation. The relaxation delay was 0.5s and the indirect dimension of each spectrum was acquired with 56 points each obtained with 704 scans. The total experimental time was 5.5 h. The rf nutation frequencies were $\nu_1 \approx 2.08$ kHz for the homonuclear recoupling sequence and 4.76 kHz for the CT-selective π and $\pi/2$ pulses. The excitation and reconversion intervals τ were equal to τ = 1280 μs. For the FAM/RAPT sequence, the rf nutation frequency was ν_1 = 60 kHz, the duration of x and $(\bar{x})$-rf pulse was τ_{pulse} = 0.85 μs and the delay between the pulse train was $\tau_{interval}$ = 0.85 μs. 30 x-$(\bar{x})$ cycles were used in the FAM/RAPT sequence.

3.3. Sensitivity to rf-inhomogeneity, C_Q and B_0 values

Another important experimental parameter is the robustness to rf-field missetting, i.e. the deviation of rf-field from the HORROR condition given by Eq. (1). The simulations were performed for the diagonal auto-peaks (Δ = 0) of the spins-5/2 system, at 18.8 T and ν_R = 15 kHz. For each recoupling sequence, the offset was fixed to the optimal value that provided the maximal sensitivity in Fig. 2. The rf-field was varied between 1.5 and 3.5 kHz in 100 Hz steps. It can be observed in Fig. 4 that the full-width at half-maximum corresponding to $BR2^1_2$ (π), is approximately 25% larger than that of $[SR2^1_4$ ($\vec{X}$)] or $[R2^1_4(\vec{X}\,\vec{X})]$ and much larger than that of $[SR2^1_2$ (π)] or $[SR4^2_4$ (π)]. Moreover, as stated above, the unbracketed sequence provides much higher sensitivity than the bracketed ones. With a full rotor sample, this lower sensitivity to rf-inhomogeneity still increases the sensitivity advantage of $BR2^1_2$ (π) over the bracketed sequences.

In Fig. 5 the 2QF efficiency of the diagonal peaks (Δ = 0), obtained for the $BR2^1_2$ (π) sequence is plotted as function of the magnetic field (Fig. 5a) and the C_Q value (Fig. 5b). In both cases, one observes an increase of efficiency with a decrease of the second-order quadrupole interaction (except for weak C_Qs in Fig. 5b, because weak rf pulses then do not rotate correctly the CT coherences).

4. Experimental verifications

As shown before, the differences between the bracketed and unbracketed sequences are more pronounced for spin-5/2 nuclei than for spin-3/2 nuclei. Aluminum-27 is a very important quadrupolar nucleus, which it is the subject of numerous publications in SS NMR. For our purpose of 2Q–1Q experiments, it has the advantage of presenting a large chemical shift difference between the tetrahedral and octahedral species, whose cross-peaks are thus difficult to excite, especially at large magnetic fields. For this reason, we have decided to focus our experimental verifications on aluminum nuclei in four different well-known $AlPO_4$ samples, namely berlinite, VPI5, $AlPO_4$-14 and CJ3. The coherence transfer pathway depicted in Fig. 1c was selected by a 64-step nested phase-cycling incrementing in $\pi/2$ steps the 2Q-excitation block, the selective π-pulse and the read-pulse, respectively [22]. We have used the States procedure for frequency sign discrimination in the 2Q indirect dimension. Other experimental parameters are indicated in the figure captions. ^{27}Al shifts in ppm are referenced to Al^{3+} (aq).

4.1. Sensitivity versus offset in berlinite

The sensitivity versus offset of the diagonal peak (Δ = 0) has been measured in a volume-restricted sample of berlinite at 18.8 T and ν_R = 15 kHz for the five selected sequences shown in Fig. 1. This compound presents a single species [35], and the 2Q–1Q spectrum thus only displays a single diagonal auto-peak. The

closest distance between two aluminum nuclei is equal to 440 pm [36], which corresponds to $b_{12} = -95$ Hz. The experimental (Fig. 6) and simulated (Fig. 2) results have very similar behavior with respect to ν_{offset}. However, experimental intensities are roughly two times smaller than simulated ones, and optimum transfer times are shorter than those predicted from numerical simulations: $\tau_{exp} \approx 1.1/1.75$ ms instead of $\tau_{sim} \approx 1.9/2.5$ ms, for bracketed/unbracketed sequences, respectively. This scaling down of intensities has been observed previously [22,25,27–29] It may be partly related to pulse transients, but it is certainly mainly related to the irreversible losses occurring during excitation and conversion periods, which also explains the shortening of the experimental transfer delays.

4.2. Sensitivity versus rf-field in berlinite

On the same restricted sample of berlinite, we have also measured the 2QF signal that can be obtained at $\nu_R = 15$ kHz for the diagonal peak ($\Delta = 0$), versus the rf-field amplitude. The relative rf-field amplitude was varied by a factor between 0.7 and 1.3 with respect to its optimal value (Fig. 7). The most robust method with respect to rf-inhomogeneity, is the unbracketed $BR2_2^1$ (π) sequence, as already shown by simulations (Fig. 4). For this method, the full-width at half-maximum ($\approx$ 1.2 kHz, $\approx \nu_{1opt}/2$) is approximately equal to its calculated value ($\approx$ 1.3 kHz: Fig. 4).

4.3. Dynamics of 0Q ↔ 2Q transfers in $AlPO_4$-VPI5

In Fig. 8 we have represented the two 2Q–1Q 2D spectra of $AlPO_4$-VPI5 recorded at 9.4T and $\nu_R = 13.5$ kHz with the same $R2_2^1$ basic recoupling scheme in its unbracketed (Fig. 8a) or bracketed (Fig. 8b) version. There are three different aluminum species in this compound: two overlapping tetrahedral sites (Al_{IV}^1 - $Al_{IV}^2 \approx 40$ ppm) and one octahedral site ($Al_{VI} \approx$ -20 ppm). The quadrupolar parameters C_Q (MHz)/η_Q of the octahedral species are 3.5/0.91 [37], and those of the tetrahedral species 1.1/0.3 (Al_{IV}^1) and 2.4/0.8 (Al_{IV}^2) [38]. The closest Al–Al distances (below 500 pm) involve pairs of distinct aluminum sites: Al_{VI}–Al_{IV}^1 (437 and 484 pm), Al_{VI}–Al_{IV}^2 (448 and 471 pm), Al_{IV}^1–Al_{IV}^2 (470 and 479 pm). The contacts between identical species are Al_{IV}^1–Al_{IV}^1 (498 pm), Al_{IV}^2–Al_{IV}^2 (521 pm) and Al_{VI}–Al_{VI} (594 pm) [39,40]. All Al–Al dipolar interactions are thus smaller than 100 Hz in absolute value. The $BR2_2^1$ sequence yields sensitivity enhancement for all peaks of 2D NMR spectra, and especially for the two cross-peaks in spite of their moderate chemical shift difference ($\Delta \approx 6$ kHz). Moreover, it can also be observed on the F_1 projection displayed versus the half-recoupling time τ (Fig. 8c) that the optimum 2Q–1Q signal is observed for a recoupling time that is c.a. three times longer when omitting the bracketing $\pi/2$ pulses. This effect, which results from the ratio of two between the scaling factors of double-quantum terms in the dipolar average Hamiltonian (see Eqs. (2) and (3)), has also been observed on berlinite. It has two opposite effects. On one hand, losses are increased during this longer transfer time. However, on the other hand it allows a fine adjustment of the recoupling time, even in case of large homonuclear dipolar interactions and/or slow spinning speeds. Indeed, the 2Q–1Q methods applied to half-integer quadrupolar nuclei accelerate by a factor of c.a. $S + 1/2$ the recoupling effect, relative that observed for spin-1/2 nuclei [25,28]. A large scaling factor can lead to a too fast build up of 2QC compared to the minimal sampling period ($4T_R$) of the recoupling intervals, and hence may reduce the 2QF signal amplitude. It should be pointed out that no cross-peaks were observed at 18.8 T and $\nu_R = 15$ kHz for the [$SR2_2^1$ (π)] sequence, whereas the $BR2_2^1$ sequence allows observing cross-peaks in such experimental conditions (not shown).

4.4. 2D 2Q–1Q spectra of $AlPO_4$-14

In Fig. 9a we have represented the 2Q–1Q 2D spectrum of as synthesized $AlPO_4$-14 recorded at 18.8 T and $\nu_R = 16$ kHz, and using $BR2_2^1$ (π) for 2QC excitation and reconversion. This compound presents four different aluminum species [41]: two tetrahedral sites (Al_3: $\delta_{cs} = 42.7$ ppm, $C_Q = 1.72$ MHz, $\eta_Q = 0.57$; Al_2: $\delta_{cs} = 43.5$ ppm, $C_Q = 3.90$ MHz, $\eta_Q = 0.83$), one pentavalent aluminum atom (Al_1: $\delta_{cs} = 27.1$ ppm, $C_Q = 5.61$ MHz, $\eta_Q = 0.93$) and one octahedral site (Al_4: $\delta_{cs} = -1.3$ ppm, $C_Q = 2.55$ MHz, $\eta_Q = 0.67$), and in addition, our sample also presents an extra-framework impurity at -2 kHz. Along with Al–O–P–O–Al connectivities, which are common for all aluminophosphate molecular sieves, in $AlPO_4$-14 there are also some Al–O–Al connectivities due to edge sharing between AlO_6 octahedra and vertex sharing between AlO_5 and AlO_6 polyhedra. The corresponding distances are 290 pm for Al_4–O–Al_4 connectivity ($b_{44} = -333$ Hz) and 360 pm for Al_1–O–Al_4 connectivity ($b_{14} = -174$ Hz) [42]. All other distances are much larger, and as an example they range over 430–480 pm ($b_{23} = -73$ to -102 Hz) between Al_2 and Al_3 nuclei.

All peaks are easily distinguishable in this figure, even the cross-peaks between tetrahedral and octahedral sites ($Al_{2,3}$–Al_4), even if they are 540 pm apart ($b_{24} = b_{34} = -52$ Hz) and display a large difference in isotropic chemical shift ($\Delta \approx 10$ kHz). The F_1 projections of the five sequences described in Fig. 1 are compared in Fig. 9b. This comparison points out the fact that the unbracketed $BR2_2^1$ (π) method gives at least a two-fold sensitivity gain over all bracketed sequences. According to simulations, this sensitivity gain would increase at $\nu_R = 30$–35 kHz (see Fig. 3d). The Al_1 autopeak is hardly visible as it corresponds to long distances (670 pm and $b_{11} = -27$ Hz) and is certainly submitted to dipolar truncation with respect to the much larger dipolar interaction ($b_{14} = -174$ Hz) between the Al_1 and Al_4 sites. This dipolar truncation, which occurs in all 2Q–1Q and 1Q–1Q homonuclear dipolar methods, is one of the most important limitations of these methods.

4.5. 2Q–1Q spectrum of $AlPO_4$-CJ3

To demonstrate the ability of the 2Q–1Q $BR2_2^1$ method to be applied even at low magnetic field, we have recorded the 2D spectrum of $AlPO_4$-CJ3, $[Al_2P_2O_8][OCH_2CH_2NH_3]$, at 7.1 T. There are two different ways of enhancing the initial ±1/2 Zeeman populations: either by saturating all populations (FAM/RAPT) [43,44] or by inverting sequentially the populations from the outer STs to the CT (DFS [45], HS [46], WURST [47]). These initial rf manipulations of the populations are not described in Fig. 1a–c. We have used the FAM/RAPT sequence, which is less efficient than the inversion methods, but more robust and which is the only method that can be used with old consoles. We obtained a signal gain of c.a. 2 on $AlPO_4$-CJ3. This sample presents two different species: one octahedral (Al_1: $C_Q(1 + \eta_Q^2/3) \approx 2.6$ MHz) and one tetrahedral site (Al_2: $C_Q(1 + \eta_Q^2/3) \approx 3.0$ MHz). The shortest Al–Al distance is between Al_1 nuclei (289 pm, $b_{11} = -336$ Hz), whereas all other distances are larger than 420 pm ($|b| < 110$ Hz) [48]. In Fig. 10 we have represented the 2Q–1Q spectrum recorded with initial FAM/RAPT and the $BR2_2^1$ sequence (Fig. 1a and d), which displays all auto- and cross-peaks with a large S/N ratio. The $BR2_2^1$ sequences gave a S/N ratio at least twice that observed with the four bracketed sequences (not shown). Moreover, in agreement with Eq. (2) and (3) its optimum contact time (1280 μs) was twice that of all bracketed sequences (640 μs).

5. Conclusions

We have demonstrated 2Q–1Q homonuclear correlation 2D experiments among the central transition of half-integer quadrupo-

lar spins with an unbracketed dipolar recoupling sequence based on the $R2_2^1$ rotor-synchronized and symmetry-based scheme initially developed for spin-1/2 nuclei. It must be noted that the super-cycling of this sequence differs from that used previously in the literature and yields higher efficiency and more robustness to rf-inhomogeneity and to offsets for auto- and cross-peaks. It allows the observation of cross-peaks that are separated by more than 10 kHz, provided the spinning speed is fast enough.

In addition to the initial enhancement of the ±1/2 Zeeman populations [43–47] three other tools can be applied to increase the signal: recycled or full echo acquisition, and slightly off-magic-angle spinning. Final recycling of the signal with CPMG train [49,50] is mostly useful when the constant time (T'_2) describing irreversible losses is large enough to be able to observe at least four or five echoes. Increasing the T'_2 value can be obtained by using fast MAS [51], which also increases the indirect spectral width of rotor-synchronized methods. As an example, by using simultaneously an initial FAM/RAPT saturation and a final CPMG recycling of the signal, a signal enhancement by a factor of c.a. 6 has been demonstrated on ^{23}Na spectra of Na_2SO_4 [23]. Another way to increase the T'_2 value is by spinning slightly off magic-angle ($\approx 0.5°$) [52]. Indeed, it has recently been shown that a signal gain of c.a. 3 could be obtained without any noticeable broadening on the second-order quadrupolar CT line-shapes [53]. When, in spite of these tools, the T'_2 value remains too small to record a sufficient number of echoes, a full echo acquisition may allow to increase the S/N ratio by a factor up to $\sqrt{2}$ [53]. Sequences described in Fig. 1a and b have then to be slightly changed for this purpose with an additional CT-selective π-pulse at the end, and the phase-cycling must be changed to select at the end the $0 \rightarrow +1 \rightarrow -1$ levels instead of the $0 \rightarrow -1$ levels as described in Fig. 1c.

When the signal is sufficient, e.g. by using the $BR2_2^1$ method with these additional tools, a high-resolution double-quantum dimension can be achieved by using high-resolution filters for half-integer quadrupolar nuclei [23]: MQMAS [54] or STMAS [55,56].

One limitation of all these sequences applied to half-integer quadrupolar nuclei is related to the fact their sensitivity curves always present one or several narrow dips, which means a careful optimization of the carrier frequency. More importantly, another limitation concerns the dipolar truncation. This means that long-range correlations between two nuclei are not visible when one of these is also involved in a short-range correlation with a third nucleus. A third limitation of all dipolar-based through-space methods is that they do not allow distinguishing between through-bond connectivity and through-space proximities. However, short recoupling times allow exciting 2QCs between the nearest-neighbor nuclei. Therefore, through-space experiments allow generally obtaining the same results as with through-bond methods, at the expense of lower S/N ratio. It must be noted that recently, several methods [58], though explicitly dealing with spin-1/2 nuclei for biological samples, are definitely exploring the same avenues than our method for quadrupolar nuclei.

Acknowledgments

Authors are grateful for funding provided by Region Nord/Pas de Calais, Europe (FEDER), CNRS, French Minister of Science, FR-3050, USTL, ENSCL, and Bruker BIOSPIN. F.D. thanks the National Natural Science Foundation of China (20773159 and 20673139) and the National Basic Research Program of China (2009CB918600) for financial support.

References

[1] S. Dusold, A. Sebald, Dipolar recoupling under magic-angle-spinning conditions, Annu. Rep. NMR Spectrosc. 41 (2000) 185–264.
[2] M.H. Levitt, in: D.M. Grant, R.K. Harris (Eds.), Symmetry-Based Pulse Sequences in Magic-Angle Spinning Solid-State NMR in Encyclopedia of Nuclear Magnetic Resonance, vol. 9, Wiley, Chichester, 2002.
[3] S. Ding, C.A. McDowell, Spectral spin diffusion of a spin-3/2 system in rotating solids, Mol. Phys. 85 (1995) 283–298.
[4] N.G. Dowell, S.E. Ashbrook, S. Wimperis, Relative orientation of quadrupole tensors from high-resolution NMR of powdered solids, J. Phys. Chem. A 106 (2002) 9470–9478.
[5] M.J. Duer, Determination of structural data from multiple-quantum magic-angle spinning NMR experiments, Chem. Phys. Lett. 277 (1997) 167–174.
[6] M.J. Duer, A.J. Painter, Correlating quadrupolar nuclear spins: a multiple-quantum NMR approach, Chem. Phys. Lett. 313 (1999) 763–770.
[7] M. Eden, L. Frydman, Quadrupolar-driven recoupling of homonuclear dipolar interactions in the nuclear magnetic resonance of rotating solids, J. Chem. Phys. 114 (2001) 4116–4123.
[8] M. Eden, J. Grinshtein, L. Frydman, High-resolution 3D exchange NMR spectroscopy and the mapping of connectivities between half-integer quadrupolar nuclei, J. Am. Chem. Soc. 124 (2002) 9708–9709.
[9] M. Eden, L. Frydman, Homonuclear NMR correlations between half-integer quadrupolar nuclei undergoing magic-angle spinning, J. Phys. Chem. B 107 (2003) 14598–14611.
[10] A.P.M. Kentgens, E.R.H. van Eck, T.G. Ajithkumar, T. Anupold, J. Past, A. Reinhold, A. Samoson, New opportunities for double rotation NMR of half-integer quadrupolar nuclei, J. Magn. Reson. 178 (2006) 212–219.
[11] I. Hung, A.P. Howes, T. Anupold, A. Samoson, D. Massiot, M.E. Smith, S.P. Brown, R. Dupree, ^{27} Al double rotation two-dimensional spin diffusion NMR: complete unambiguous assignment of aluminum sites in $9Al_2O_3{\cdot}2B_2O_3$, Chem. Phys. Lett. 432 (2006) 152–156.
[12] A. Vinu, K. Ariga, T. Mori, K. Takegoshi, Two dimensional ^{11}B–^{11}B exchange NMR study in mesoporous boron carbon nitride at 21.8 T, Solid State Nucl. Magn. Reson. 31 (2007) 193–196.
[13] M. Nijman, M. Ernst, A.P.M. Kentgens, B.H. Meier, Rotational-resonance NMR experiments in half-integer quadrupolar spin-systems, Mol. Phys. 98 (2000) 161–178.
[14] P. Hartmann, C. Jäger, J.W. Zwanziger, Off-angle correlation spectroscopy applied to spin-1/2 and quadrupolar nuclei, Solid State Nucl. Magn. Reson. 13 (1999) 245–254.
[15] T.G. Ajithkumar, A.P.M. Kentgens, Homonuclear correlation experiments of half-integer quadrupolar nuclei using multiple-quantum techniques spinning at a P_4 magic angle, J. Am. Chem. Soc. 125 (2003) 2398–2399.
[16] S. Vega, Fictitious spin-1/2 operator formalism for multiple quantum NMR, J. Chem. Phys. 68 (1978) 5518–5527.
[17] T.G. Oas, R.G. Griffin, M.H. Levitt, Rotary resonance recoupling of dipolar interactions in solid-state nuclear magnetic resonance spectroscopy, J. Chem. Phys. 89 (1988) 692–695.
[18] N.C. Nielsen, H. Bildsoe, H.J. Jakobsen, M.H. Levitt, Double-quantum homonuclear rotary resonance: efficient dipolar recovery in magic-angle spinning nuclear magnetic resonance, J. Chem. Phys. 101 (1994) 1805–1812.
[19] M. Baldus, D. Rovnyak, R.G. Griffin, Radio-frequency-mediated dipolar recoupling among half-integer quadrupolar spins, J. Chem. Phys. 112 (2000) 5902–5909.
[20] S. Wi, J.W. Logan, D. Sakellariou, J.D. Walls, A. Pines, Rotary resonance recoupling for half-integer quadrupolar nuclei in solid-state nuclear magnetic resonance spectroscopy, J. Chem. Phys. 117 (2002) 7024–7033.
[21] J. Painter, M.J. Duer, Double-quantum-filtered nuclear magnetic resonance spectroscopy applied to quadrupolar nuclei in solids, J. Chem. Phys. 116 (2002) 710–722.
[22] G. Mali, G. Fink, F. Taulelle, Double-quantum homonuclear correlation magic-angle sample spinning nuclear magnetic resonance spectroscopy of dipolar-coupled quadrupolar nuclei, J. Chem. Phys. 120 (2004) 2835–2845.
[23] G. Mali, V. Kaucic, Enhancing sensitivity or resolution of homonuclear correlation experiment for half-integer quadrupolar nuclei, J. Magn. Reson. 171 (2004) 48–56.
[24] M. Eden, H. Annersten, A. Zazzi, Pulse-assisted homonuclear dipolar recoupling of half-integer quadrupolar spins in magic-angle spinning NMR, Chem. Phys. Lett. 410 (2005) 24–30.
[25] M. Eden, D. Zhou, J. Yu, Improved double-quantum NMR correlation spectroscopy of dipolar-coupled quadrupolar spins, Chem. Phys. Lett. 431 (2006) 397–403.
[26] M.R. Hansen, H.J. Jakobsen, J. Skibsted, Structural environments for boron and aluminum in alumina-boria catalysts and their precursors from ^{11}B and ^{27}Al single- and double-resonance MAS NMR experiments, J. Phys. Chem. C112 (2008) 7210–7222.
[27] A.Y.H. Lo, M. Eden, Efficient symmetry-based homonuclear dipolar recoupling of quadrupolar spins: double-quantum NMR correlations in amorphous solids, Phys. Chem. Chem. Phys. 10 (2008) 6635–6644.
[28] G. Mali, V. Kaucic, F. Taulelle, Measuring distances between half-integer quadrupolar nuclei and detecting relative orientations of quadrupolar and dipolar tensors by double-quantum homonuclear dipolar recoupling nuclear magnetic resonance experiments, J. Chem. Phys. 128 (2008) 204503.
[29] A. Brinkmann, A.P.M. Kentgens, T. Anupold, A. Samoson, Symmetry-based recoupling in double-rotation NMR spectroscopy, J. Chem. Phys. 129 (2008) 174507.
[30] M. Carravetta, M. Edén, X. Zhao, A. Brinkmann, M.H. Levitt, Symmetry principles for the design of radiofrequency pulse sequences in the nuclear magnetic resonance of rotating solids, Chem. Phys. Lett. 321 (2000) 205–215.

[31] A. Brinkmann, M. Eden, Second order average Hamiltonian theory of symmetry-based pulse schemes in the nuclear magnetic resonance of rotating solids: application to triple-quantum dipolar recoupling, J. Chem. Phys. 120 (2004) 11726–11745.
[32] A. Brinkmann, J. Schmedt auf der Günne, M.H. Levitt, Homonuclear zero-quantum recoupling in fast magic-angle spinning nuclear magnetic resonance, J. Magn. Reson. 156 (2002) 79–96.
[33] M. Bak, J.T. Rasmussen, N.C. Nielsen, SIMPSON: a general simulation program for solid-state NMR spectroscopy, J. Magn. Reson. 147 (2000) 296–330.
[34] M. Bak, N.C. Nielsen, REPULSION: a novel approach to efficient powder averaging in solid-state NMR, J. Magn. Reson. 125 (1997) 132–139.
[35] D. Massiot, F. Fayon, B. Alonso, J. Trebosc, J.P. Amoureux, Chemical bonding differences evidenced from *J*-coupling in solid-state NMR experiments involving quadrupolar nuclei, J. Magn. Reson. 164 (2003) 160–164.
[36] A. Goiffon, J.C. Jumas, M.M. Aurin, E. Philippot, J. Solid State Chem. 61 (1986) 384–396.
[37] J. Rocha, W. Kolodziejski, H. He, J. Klinowski, Solid state NMR studies of hydrated porous aluminophosphate VPI-5, J. Am. Chem. Soc. 114 (1992) 4884–4888.
[38] J. Rocha, A.P. Esculcas, C. Fernandez, J.P. Amoureux, 2D triple-quantum ^{27}Al MAS NMR spectroscopy study of the high-temperature phase transformation of microporous VPI-5, J. Phys. Chem. 100 (1996) 17889.
[39] L.B. McCusker, Ch. Barlocher, E. Jahn, M. Bulow, Zeolites 11 (1991) 308.
[40] E.G. Derouane, H. He, S.B. Derouane-Abd Hamid, I.I. Ivanova, In situ MAS NMR investigations of molecular sieves and zeolite-catalyzed reactions, Catal. Lett. 58 (1999) 1–19.
[41] C. Fernandez, J.P. Amoureux, C. Chezeau, L. Delmotte, A. Kessler, Al-MAS NMR characterization of $AlPO_4$-14. Enhanced resolution and information by MQMAS, Microporous Mater. 6 (1996) 331–340.
[42] R.W. Broach, S.T. Wilson, R.M. Kirchner, Corrected crystallographic tables and figure for as-synthesized $AlPO_4$-14, Microporous Mesoporous Mater. 57 (2003) 211–214.
[43] P.K. Madhu, A. Golbourt, L. Frydman, S. Vega, Sensitivity enhancement of the MQMAS NMR experiment by fast amplitude modulation of the pulses, Chem. Phys. Lett. 307 (1999) 41–47.
[44] Z. Yao, H.T. Kwak, D. Sakellariou, L. Emsley, P.J. Grandinetti, Sensitivity enhancement of the central transition NMR signal of quadrupolar nuclei under magic-angle spinning, Chem. Phys. Lett. 327 (2001) 85–90.
[45] A.P.M. Kentgens, R. Verhagen, Advantages of double-frequency sweeps in static, MAS and MQMAS NMR of spin-3/2 nuclei, Chem. Phys. Lett. 300 (1999) 435–443.
[46] R. Siegel, T.T. Nakashima, R.E. Wasylishen, Signal enhancement of NMR spectra of half-integer quadrupolar nuclei in solids using hyperbolic secant pulses, Chem. Phys. Lett. 388 (2004) 441–445.
[47] K.K. Dey, S. Prasad, J.T. Ash, M. Deschamps, P.J. Grandinetti, Spectral editing in solid state MAS NMR of quadrupolar nuclei using selective satellite inversion, J. Magn. Reson. 185 (2007) 326–330.
[48] K. Wang, J. Yu, G. Zhu, Y. Zou, R. Xu, Synthesis and characterization of a new microporous aluminophosphate $[Al_2P_2O_8][OCH_2CH_2NH_3]$ with an open-framework analogous to $AlPO_4$-D, Microporous Mesoporous Mater. 39 (2000) 281–289.
[49] T. Vosegaard, F.H. Larsen, H.J. Jakobsen, P.D. Ellis, N.C. Nielsen, Sensitivity-enhanced multiple quantum MAS NMR of half-integer quadrupolar nuclei, J. Am. Chem. Soc. 119 (1997) 9055–9056.
[50] R. Lefort, J. W Wiench, M. Pruski, J.P. Amoureux, Optimization of data acquisition and processing in Carr–Purcell–Meiboom–Gill multiple-quantum magic angle spinning nuclear magnetic resonance, J. Chem. Phys. 116 (2002) 2493–2501.
[51] K. Mao, J. Wiench, V.S.Y. Lin, M. Pruski, Indirectly detected through-bond chemical shift correlation NMR spectroscopy in solids under fast MAS: studies of organic-inorganic hybrid materials, J. Magn. Reson. 196 (2009) 92–95.
[52] H.T. Kwak, P. Srinivasan, J. Quine, D. Massiot, Z. Gan, Satellite transition rotational resonance of homonuclear quadrupolar spins: magic-angle effect on spin-echo decay and inversion recovery, Chem. Phys. Lett. 376 (2003) 75–82.
[53] D. Iuga, C. Morais, Z. Gan, D.R. Neuville, L. Cormier, D. Massiot, NMR heteronuclear correlation between quadrupolar nuclei in solids, J. Am. Chem. Soc. 127 (2005) 11540–11541.
[54] L. Frydman, J.S. Harwood, Isotropic spectra of half-integer quadrupolar spins from bidimensional magic-angle spinning NMR, J. Am. Chem. Soc. 117 (1995) 5367–5368.
[55] Z. Gan, Isotropic NMR spectra of half-integer quadrupolar nuclei using satellite transitions and magic-angle spinning, J. Am. Chem. Soc. 122 (2000) 3242–3243.
[56] J. Trebosc, J.P. Amoureux, Z. Gan, Comparison of high-resolution solid-state NMR MQMAS and STMAS methods for half-integer quadrupolar nuclei, Solid State NMR 31 (2007) 1–9.
[57] M. Edén, Determination of absolute quadrupolar tensor orientations by double-quantum NMR on powders, Chem. Phys. Lett. 470 (2009) 318–324.
[58] J. Lin, M.J. Bayro, R.G. Griffin, N. Khaneja, Dipolar recoupling in solid state NMR by phase alternating pulse sequences, J. Magn. Reson. 197 (2009) 145–152.